

Numerical solution of an inverse medium scattering problem for Maxwell's Equations at fixed frequency

Gang Bao^{a,1}, Peijun Li^{b,*,2}

^a Department of Mathematics, Michigan State University, East Lansing, MI 48824, United States

^b Department of Mathematics, Purdue University, West Lafayette, IN 47907, United States

ARTICLE INFO

Article history:

Received 29 August 2008

Received in revised form 19 March 2009

Accepted 20 March 2009

Available online 1 April 2009

PACS:

02.30.Zz

41.20.Jb

Keywords:

Inverse medium scattering

Maxwell's equations

Near-field optics

Recursive linearization

Evanescent plane waves

ABSTRACT

Consider a time-harmonic electromagnetic plane wave incident on a medium enclosed by a bounded domain in \mathbb{R}^3 . In this paper, well-posedness of the variational problem for the direct scattering is examined. An energy estimate for the scattered field is obtained on which the Born approximation is based. A regularized recursive linearization method for the inverse medium scattering, which reconstructs the scatterer of an inhomogeneous medium from the boundary measurements of the scattered field, is developed. The algorithm requires only single-frequency data. Using an initial guess from the Born approximation, each update is obtained via continuation on the spatial frequency of a two-parameter family of plane waves by solving one direct problem and one adjoint problem of the Maxwell equation.

Published by Elsevier Inc.

1. Introduction

Consider the system of time-harmonic Maxwell's equations in three dimensions

$$\operatorname{curl} \mathbf{E} = i\omega \mu \mathbf{H}, \quad (1)$$

$$\operatorname{curl} \mathbf{H} = -i\omega \varepsilon \mathbf{E}, \quad (2)$$

where \mathbf{E} and \mathbf{H} are the total electric field and magnetic field, ω is the angular frequency, ε is the electric permittivity and μ is the magnetic permeability. Denote by ε_0 and μ_0 the permittivity and permeability of the vacuum. The fields are further assumed to be nonmagnetic, i.e., $\mu = \mu_0$. Rewrite $\varepsilon = \varepsilon_0 \varepsilon_r$ and $\varepsilon_r = 1 + q$ is the relative permittivity, where q is the scatterer and is assumed to be supported in the ball $B = \{\mathbf{x} \in \mathbb{R}^3 : |\mathbf{x}| < \rho\}$ of radius ρ with the surface $S = \{\mathbf{x} \in \mathbb{R}^3 : |\mathbf{x}| = \rho\}$. Throughout this paper, we assume for simplicity in exposition that $\varepsilon_0 = 1$, $\mu_0 = 1$ and $\rho = 1$.

Taking the curl of Eq. (1) and eliminating the magnetic field from Eq. (2), we obtain the uncoupled equation for the total electric field

* Corresponding author.

E-mail addresses: bao@math.msu.edu (G. Bao), lpeijun@math.purdue.edu (P. Li).

¹ The research was supported in part by the NSF grants DMS-0604790, CCF-0514078, EAR-0724527, and the ONR grant N000140210365.

² The research was supported in part by the NSF EAR-0724656.

$$\text{curl curl } \mathbf{E} - \kappa^2(1 + q)\mathbf{E} = 0, \tag{3}$$

where $\kappa = \omega\sqrt{\epsilon_0\mu_0}$ is the wavenumber.

Given two real numbers η_1 and η_2 , denote the transverse wave vector $\boldsymbol{\eta} = (\eta_1, \eta_2)$ and the wave vector $\mathbf{k} = (\boldsymbol{\eta}, k(\boldsymbol{\eta}))$, where

$$k(\boldsymbol{\eta}) = \begin{cases} \sqrt{\kappa^2 - |\boldsymbol{\eta}|^2} & \text{for } \kappa > |\boldsymbol{\eta}|, \\ i\sqrt{|\boldsymbol{\eta}|^2 - \kappa^2} & \text{for } \kappa < |\boldsymbol{\eta}|. \end{cases}$$

Here $|\boldsymbol{\eta}| = \sqrt{\eta_1^2 + \eta_2^2}$ is known as the spatial frequency. Equivalently, the transverse wave vector can be written in the polar form $\boldsymbol{\eta} = (|\boldsymbol{\eta}|\cos\theta, |\boldsymbol{\eta}|\sin\theta)$, where $\theta \in [0, 2\pi]$ is the angle. The scatterer is illuminated by a two-parameter family of plane waves

$$\mathbf{E}^{\text{in}} = \mathbf{p}e^{i\mathbf{k}\cdot\mathbf{x}}, \tag{4}$$

or in an explicit form

$$\mathbf{E}^{\text{in}} = \begin{cases} \mathbf{p}e^{i(\eta_1x_1 + \eta_2x_2)} e^{i\sqrt{\kappa^2 - |\boldsymbol{\eta}|^2}x_3} & \text{for } \kappa > |\boldsymbol{\eta}|, \\ \mathbf{p}e^{i(\eta_1x_1 + \eta_2x_2)} e^{-\sqrt{|\boldsymbol{\eta}|^2 - \kappa^2}x_3} & \text{for } \kappa < |\boldsymbol{\eta}|. \end{cases}$$

where \mathbf{p} is the polarization vector satisfying $\mathbf{p} \cdot \mathbf{k} = 0$.

The modes for which $|\boldsymbol{\eta}| < \kappa$ correspond to propagating plane waves while the modes with $|\boldsymbol{\eta}| > \kappa$ correspond to evanescent plane waves. Therefore, the illuminating field consists of high spatial frequency evanescent plane waves and propagating plane waves. Evanescent plane waves may be generated at the interface of two media by total internal reflection [9,10], which has been in practical use primarily in near-field optics [17]. A recent review on the near-field microscopy and near-field optics may be found in [16,22]. These waves are oscillatory parallel to the x_1x_2 -plane and decay exponentially along the x_3 -axis. The higher the spatial frequency of the evanescent plane waves used to probe the scatterer is, the more rapidly the field decays as a function of depth into the scatterer. Evidently, such an incident wave satisfies the homogeneous equation

$$\text{curl curl } \mathbf{E}^{\text{in}} - \kappa^2\mathbf{E}^{\text{in}} = 0. \tag{5}$$

Note 1. Strictly speaking, the evanescent plane waves given in Eq. (4) decay only in $\mathbb{R}_+^3 = \{\mathbf{x} \in \mathbb{R}^3 : x_3 > 0\}$. However, without the loss of generality, we may assume that the scatterer is located in the \mathbb{R}_+^3 .

The total electric field \mathbf{E} consists of the incident field \mathbf{E}^{in} and the scattered field \mathbf{E}^{sc} :

$$\mathbf{E} = \mathbf{E}^{\text{in}} + \mathbf{E}^{\text{sc}}.$$

It follows from Eqs. (3) and (5) that the scattered field satisfies

$$\text{curl curl } \mathbf{E}^{\text{sc}} - \kappa^2(1 + q)\mathbf{E}^{\text{sc}} = \kappa^2q\mathbf{E}^{\text{in}}. \tag{6}$$

Note 2. In this paper, we adopt the non-global approach, i.e., the scattered field resulting from the interaction of the incident field with the sample is analyzed in the absence of other medium or the tip. In this case, the scattering problem may be formulated in the free space. The global approach which takes into account the entire system is a subject of future work.

In the free space, the scattered field is required to satisfy the following Silver–Müller radiation condition:

$$\lim_{|\mathbf{x}| \rightarrow \infty} (\text{curl } \mathbf{E}^{\text{sc}} \wedge \mathbf{x} - ik|\mathbf{x}|\mathbf{E}^{\text{sc}}) = 0, \tag{7}$$

uniformly along all directions $\mathbf{x}/|\mathbf{x}|$.

Two mathematical problems emerge: the direct scattering problem and the inverse scattering problem. The *direct problem* is to determine the scattered field \mathbf{E}^{sc} , given the incident field \mathbf{E}^{in} and the scatterer $q(\mathbf{x})$. In this work, based on a Hodge decomposition and a compact imbedding result, the direct problem is shown to have a unique solution for all but possibly a discrete set of wavenumbers. Furthermore, an energy estimate for the scattered field is given, which provides a theoretical basis for our linearization algorithm. For numerical solution of the direct scattering problem, the reader is referred to [28–30] and references therein. See also [32,37] for detailed analysis of the solutions of the Maxwell system.

Given a two-parameter family of incident plane waves \mathbf{E}^{in} , the *inverse problem* is to reconstruct the scatterer $q(\mathbf{x})$ from the boundary measurement of the corresponding scattered field \mathbf{E}^{sc} . Here the scattered field is measured by an idealized point detector at $\mathbf{x}_j \in S, j = 1, \dots, J$. The boundary measurement could be of full aperture, i.e., the scattered field is measured all around the sphere S , or the measurement could be of limited aperture, i.e., the scattered field is only available on a part of the sphere, e.g. upper part of the sphere S . The inverse scattering problems arise naturally in diverse applications such

as radar and sonar, geophysical exploration, medical imaging and nondestructive testing [14,33]. However, work in this area has only recently progressed from a collection of ad-hoc techniques with little rigorous mathematical basis to the forefront of mathematical research in scattering theory. The reason is that the inverse problem is inherently nonlinear and, more seriously from the computational point of view, ill-posed. In particular, small variations in the measured data can lead to large errors in the reconstruction. In addition to nonlinearity and ill-posedness, difficulties arise from the possible use of limited aperture data, which makes the ill-posedness and nonlinearity of the inverse problem even more severe. Of course, the large scale computation always presents a challenge for computational inverse problems, especially in the three-dimensional case.

The original direct and inverse problems are imposed in the open domain. In practice, the open domain needs to be truncated into a bounded domain. Therefore, a suitable boundary condition has to be imposed on the boundary of the bounded domain so that no artificial wave reflection occurs. There are a variety of ways to provide such boundary conditions, e.g. non-local Dirichlet-to-Neumann (DtN) maps, local absorbing boundary conditions as approximations to nonlocal DtN maps, and perfectly matched layer techniques. The analysis of the direct problem is based on a reduced boundary value problem in a ball via a capacity operator, i.e., a DtN map, while a first order absorbing boundary condition is employed numerically for solving both the direct and inverse problems, i.e., synthetic data and reconstructions are based on an approximate problem. Though we employed the same numerical method for solving the direct problem to creating the data and inversion, no inverse crime is committed here since the scattered fields are computed from different meshes and are perturbed by random noise.

Our main goal of the work is to present a novel computational approach for solving the three-dimensional inverse medium problems with full or limited aperture data. In [11,3], stable and efficient continuation methods with respect to the wavenumber were proposed for solving the two-dimensional Helmholtz equation and three-dimensional Maxwell's equations, respectively, in the case of full aperture data. A homotopy continuation method with limited aperture data may be found in [7]. These approaches require multiple frequency scattering data and are based on the recursive linearization along wavenumbers. For the two-dimensional inverse medium problems with fixed frequency scattering data, new continuation approach was proposed in [12] in the case of a spherically symmetric medium and spherical incident waves, and more recently in [4] by using evanescent plane waves. We refer the reader to [5,6,13,18,24,25,34,35,39] for related results on the inverse scattering problem. See [14,15] for an account of recent progress on the general inverse scattering problem. Although our present approach may be viewed as an extension from our previous work [4] for solving the inverse scattering problem for the two-dimensional Helmholtz equations at fixed frequency, there are significant differences. The illuminating fields used in this paper including the high spatial frequency evanescent plane waves are a two-parameter family of plane waves. The recursive linearization is obtained by a continuation on the spatial frequency of the incident waves from solutions of one direct problem and one adjoint problem of the Maxwell equations.

The paper is organized as follows. Analysis of the variational problem for the direct scattering is presented in Section 2. In particular, the well-posedness of the direct problem is proved and an energy estimate is given. In Section 3, an initial guess of the reconstruction is derived systematically from the Born approximation in the case of weak scattering. A regularized recursive linearization method and its numerical examples are presented in Sections 4 and 5, respectively. The paper is concluded with some remarks and future directions in Section 6.

2. Energy estimate

In this section, the variational formulation for the direct scattering is examined to provide criteria for weak scattering, which plays an important role in the inversion method.

For any smooth vector field \mathbf{u} , denote by \mathbf{u}_S its tangential component on the surface S :

$$\mathbf{u}_S = -(\mathbf{u} \wedge \mathbf{n}) \wedge \mathbf{n},$$

where \mathbf{n} is the unit outer normal vector to S . Introduce the following usual functional spaces:

$$\begin{aligned} H_0^1(B) &= \{\zeta \in H^1(B), \zeta = 0 \text{ on } S\}, \\ H(\text{curl}, B) &= \{\mathbf{u} \in (L^2(B))^3, \text{curl } \mathbf{u} \in (L^2(B))^3\}, \\ TL^2(S) &= \{\mathbf{u} \in (L^2(S))^3, \mathbf{u} \cdot \mathbf{n} = 0\}, \\ TH^{-1/2}(\text{curl}, S) &= \{\mathbf{u} \in (H^{-1/2}(S))^3, \mathbf{u} \cdot \mathbf{n} = 0, \text{curl}_S \mathbf{u} \in H^{-1/2}(S)\}, \\ TH^{-1/2}(\text{div}, S) &= \{\mathbf{u} \in (H^{-1/2}(S))^3, \mathbf{u} \cdot \mathbf{n} = 0, \text{div}_S \mathbf{u} \in H^{-1/2}(S)\}. \end{aligned}$$

For the definitions of the scalar rotational curl_S and the surface divergence div_S , we refer to [37]. Recall that the two spaces $TH^{-1/2}(\text{curl}, S)$ and $TH^{-1/2}(\text{div}, S)$ are mutually adjoint with respect to the scalar product in $TL^2(S)$, i.e., $TH^{-1/2}(\text{curl}, S) = TH^{-1/2}(\text{div}, S)$.

To reformulate the problem from open domain into a bounded domain, we introduce the capacity operator \mathcal{T} [2]. Let $Y_n^m(\theta, \varphi)$ be an orthonormal sequence of spherical harmonics on the unit sphere that satisfy

$$\Delta_S Y_n^m + n(n+1)Y_n^m = 0,$$

where Δ_S is the Laplace–Beltrami operator on S . Let ∇_S be the surface tangential gradient on S . Then an orthonormal basis for $TL^2(S)$ consists of functions of the form

$$\mathbf{V}_n^m = \frac{1}{\sqrt{n(n+1)}} \nabla_S Y_n^m \quad \text{and} \quad \mathbf{U}_n^m = \mathbf{V}_n^m \wedge \mathbf{n}.$$

It follows that any tangential vector field $\mathbf{u} \in TL^2(S)$ may be represented as

$$\mathbf{u} = \sum_{n=1}^{\infty} \sum_{m=-n}^n [\alpha_n^m \mathbf{U}_n^m + \beta_n^m \mathbf{V}_n^m].$$

The explicit representation of the capacity operator \mathcal{T} can be written

$$\mathcal{T}\mathbf{u} = \sum_{n=1}^{\infty} \sum_{m=-n}^n \left[\frac{\alpha_n^m \gamma_n(\kappa)}{i\kappa} \mathbf{U}_n^m + \frac{i\kappa \beta_n^m}{\gamma_n(\kappa)} \mathbf{V}_n^m \right],$$

where

$$\gamma_n(\kappa) = 1 + \kappa \frac{h_n^{(1)'(\kappa)}}{h_n^{(1)}(\kappa)},$$

and $h_n^{(1)}$ is the Hankel function of the first kind of order n .

Using the capacity operator \mathcal{T} , the problem (6) and (7) can be reduced to one in a bounded domain:

$$\text{curl curl } \mathbf{E}^{\text{sc}} - \kappa^2(1+q)\mathbf{E}^{\text{sc}} = \kappa^2 q \mathbf{E}^{\text{in}} \quad \text{in } B, \tag{8}$$

$$\text{curl } \mathbf{E}^{\text{sc}} \wedge \mathbf{n} - i\kappa \mathcal{T} \mathbf{E}_S^{\text{sc}} = \mathbf{0} \quad \text{on } S. \tag{9}$$

Multiplying Eq. (8) by a test function $\mathbf{F} \in H(\text{curl}, B)$, integrating over B , and using integration by parts, we arrive at the variational form for the scattering problem (8) and (9): Find $\mathbf{E}^{\text{sc}} \in H(\text{curl}, B)$ such that

$$a(\mathbf{E}^{\text{sc}}, \mathbf{F}) = b(\mathbf{F}) \quad \text{for all } \mathbf{F} \in H(\text{curl}, B), \tag{10}$$

where the bilinear form

$$a(\mathbf{u}, \mathbf{v}) = \int_B \text{curl } \mathbf{u} \cdot \text{curl } \bar{\mathbf{v}} - \kappa^2 \int_B (1+q) \mathbf{u} \cdot \bar{\mathbf{v}} - i\kappa \int_S \mathcal{T} \mathbf{u}_S \cdot \bar{\mathbf{v}}_S \tag{11}$$

and the functional

$$b(\mathbf{v}) = \kappa^2 \int_B q \mathbf{E}^{\text{in}} \cdot \bar{\mathbf{v}}. \tag{12}$$

Throughout the paper, C stands for a positive generic constant whose value may change but should always be clear from the context. Before presenting the main theorem for the variational problem, we state a useful imbedding result. The reader is referred to [1] for a detailed discussion and proof.

Lemma 1. *Let W be a functional space defined by*

$$W = \{ \mathbf{u} \in H(\text{curl}, B) : \text{div}((1+q)\mathbf{u}) = 0 \text{ in } B \text{ and } (1+q)\mathbf{u} \cdot \mathbf{n} = \frac{i}{\kappa} \text{div}_S \mathcal{T} \mathbf{u}_S \text{ on } S \}.$$

The embedding from W to $(L^2(B))^3$ is compact.

Next we prove the well-posedness of the variational problem (10) and obtain an energy estimate for the scattered field.

Theorem 1. *Given a scatterer $q \in L^\infty(B)$, for all but possibly a discrete set of wavenumbers κ , the variational problem (10) admits a unique weak solution in $H(\text{curl}, B)$, given by $\mathbf{E}^{\text{sc}} = \mathbf{u} + \nabla p$, while $\mathbf{u} \in W, p \in H_0^1(B)$. Furthermore, there exists a constant C such that the following estimate holds:*

$$\| \mathbf{E}^{\text{sc}} \|_{H(\text{curl}, B)} \leq C \| q \|_{L^\infty(B)} \| \mathbf{E}^{\text{in}} \|_{(L^2(B))^3}. \tag{13}$$

Proof. Using the Hodge decomposition, we take $\mathbf{E}^{\text{sc}} = \mathbf{u} + \nabla \zeta$ and $\mathbf{F} = \mathbf{v} + \nabla \xi$ for any $\mathbf{v} \in W$ and $\xi \in H_0^1(B)$. Observe that $a(\mathbf{u}, \nabla \xi) = 0$ by the definition of W . Therefore, we decompose the variational Eq. (10) into the form

$$a(\mathbf{u}, \mathbf{v}) + a(\nabla \zeta, \mathbf{v}) + a(\nabla \zeta, \nabla \xi) = b(\mathbf{v}) + b(\nabla \xi) \quad \text{for all } \mathbf{v} \in W \text{ and } \xi \in H_0^1(B). \tag{14}$$

First we determine $\zeta \in H_0^1(B)$ by the solution of

$$a(\nabla \zeta, \nabla \xi) = b(\nabla \xi) \quad \text{for all } \xi \in H_0^1(B),$$

which gives explicitly

$$\int_B (1+q) \nabla \zeta \cdot \nabla \bar{\xi} = - \int_B q \mathbf{E}^{\text{in}} \cdot \nabla \bar{\xi} \quad \text{for all } \xi \in H_0^1(B).$$

The existence and uniqueness of the solution ζ in $H_0^1(B)$ may be proved by a direct application of the Lax–Milgram lemma with the estimate

$$\|\nabla\zeta\|_{(L^2(B))^3} \leq C\|q\|_{L^\infty(B)}\|\mathbf{E}^{\text{in}}\|_{(L^2(B))^3}. \tag{15}$$

Rewrite Eq. (14) as

$$a(\mathbf{u}, \mathbf{v}) = b(\mathbf{v}) - a(\nabla\zeta, \mathbf{v}) \quad \text{for all } \mathbf{v} \in W, \tag{16}$$

and decompose the bilinear form a into

$$a = a_1 - \kappa^2 a_2,$$

where

$$\begin{aligned} a_1(\mathbf{u}, \mathbf{v}) &= \int_B \text{curl } \mathbf{u} \cdot \text{curl } \bar{\mathbf{v}} - i\kappa \int_S \mathcal{T}\mathbf{u}_S \cdot \bar{\mathbf{v}}_S, \\ a_2(\mathbf{u}, \mathbf{v}) &= \int_B (1 + q)\mathbf{u} \cdot \bar{\mathbf{v}}. \end{aligned}$$

We conclude from the non-negative property of the capacity operator \mathcal{T} [37] that a_1 is coercive:

$$|a_1(\mathbf{u}, \mathbf{u})| \geq C\|\mathbf{u}\|_{H(\text{curl}, B)}^2 \quad \text{for all } \mathbf{v} \in W.$$

The continuity of the bilinear form a_1 follows from the Cauchy–Schwarz inequality.

Next we prove the compactness of a_2 . Define an operator $\mathcal{A} : (L^2(B))^3 \rightarrow W$ by

$$a_1(\mathcal{A}\mathbf{u}, \mathbf{v}) = a_2(\mathbf{u}, \mathbf{v}) \quad \text{for all } \mathbf{v} \in W,$$

which gives

$$\int_B \text{curl } \mathcal{A}\mathbf{u} \cdot \text{curl } \bar{\mathbf{v}} - i\kappa \int_S \mathcal{T}\mathcal{A}\mathbf{u}_S \cdot \bar{\mathbf{v}}_S = \int_B (1 + q)\mathbf{u} \cdot \bar{\mathbf{v}} \quad \text{for all } \mathbf{v} \in W.$$

From the Lax–Milgram lemma again, it follows that

$$\|\mathcal{A}\mathbf{u}\|_{H(\text{curl}, B)} \leq C\|\mathbf{u}\|_{(L^2(B))^3}. \tag{17}$$

Thus \mathcal{A} is bounded from $(L^2(B))^3$ to W and W is compactly imbedded into $(L^2(B))^3$. Hence $\mathcal{A} : (L^2(B))^3 \rightarrow (L^2(B))^3$ is a compact operator.

Define a function $\mathbf{w} \in (L^2(B))^3$ satisfying

$$a_1(\mathbf{w}, \mathbf{v}) = b(\mathbf{v}) - a(\nabla\zeta, \mathbf{v}) \quad \text{for all } \mathbf{v} \in W.$$

More specifically, we have by using the Stokes formula that

$$a_1(\mathbf{w}, \mathbf{v}) = \kappa^2 \int_B q\mathbf{E}^{\text{in}} \cdot \bar{\mathbf{v}} + \kappa^2 \int_B (1 + q)\nabla\zeta \cdot \bar{\mathbf{v}} \quad \text{for all } \mathbf{v} \in W.$$

It follows from the Lax–Milgram lemma that

$$\|\mathbf{w}\|_{H(\text{curl}, B)} \leq C\|q\|_{L^\infty(B)}\|\mathbf{E}^{\text{in}}\|_{(L^2(B))^3} + C\|\nabla\zeta\|_{(L^2(B))^3}.$$

An application of estimate (15) yields

$$\|\mathbf{w}\|_{H(\text{curl}, B)} \leq C\|q\|_{L^\infty(B)}\|\mathbf{E}^{\text{in}}\|_{(L^2(B))^3}. \tag{18}$$

Using the operator \mathcal{A} , we can see that the problem (16) is equivalent to finding $\mathbf{u} \in (L^2(B))^3$ such that

$$(\mathcal{T} - \kappa^2\mathcal{A})\mathbf{u} = \mathbf{w}. \tag{19}$$

It follows from the Fredholm alternative that there exists a unique solution of (19) for all but possibly a discrete set of wave-number κ . We then have the estimate

$$\|\mathbf{u}\|_{(L^2(B))^3} \leq C\|\mathbf{w}\|_{(L^2(B))^3}. \tag{20}$$

Rearranging Eq. (19), we have $\mathbf{u} = \mathbf{w} - \kappa^2\mathcal{A}\mathbf{u}$, so $\mathbf{u} \in W$ and, by the estimate (17) for the operator \mathcal{A} , we have

$$\|\mathbf{u}\|_{H(\text{curl}, B)} \leq C\|\mathbf{w}\|_{H(\text{curl}, B)} + C\|\mathbf{u}\|_{(L^2(B))^3}.$$

Combining the estimates (18) and (20) leads to

$$\|\mathbf{u}\|_{H(\text{curl}, B)} \leq C\|q\|_{L^\infty(B)}\|\mathbf{E}^{\text{in}}\|_{(L^2(B))^3}. \tag{21}$$

Finally, it follows from the definition of the norm in $H(\text{curl}, B)$ that

$$\|\mathbf{E}^{\text{sc}}\|_{H(\text{curl}, B)} \leq \|\mathbf{u}\|_{H(\text{curl}, B)} + \|\nabla\zeta\|_{(L^2(B))^3}.$$

The proof is complete by noting the estimates (15) and (21). \square

Note 3. Using the explicit form of the evanescent plane wave (4) with $|\eta| > \kappa$, the estimate (13) can be written as

$$\|\mathbf{E}^{\text{sc}}\|_{H(\text{curl}, B)} \leq C(|\eta|^2 - \kappa^2)^{-1/4} \|q\|_{L^\infty(B)}, \tag{22}$$

where the constant C depends on κ . The above energy estimate provides a criterion for the weak scattering. For a fixed wave-number κ and a scatterer q , the scattered field is weak if the spatial frequency of the incident wave $|\eta|$ is large.

3. Born approximation

In this section, we discuss how to generate an initial guess for the proposed iteratively recursive linearization method based on the Born approximation.

Rewrite Eq. (8) as

$$\text{curl curl } \mathbf{E}^{\text{sc}} - \kappa^2 \mathbf{E}^{\text{sc}} = \kappa^2 q (\mathbf{E}^{\text{in}} + \mathbf{E}^{\text{sc}}). \tag{23}$$

From the energy estimate (22), the scattered field is weak when the spatial frequency $|\eta|$ is large. By dropping the scattered field at the right hand side of Eq. (23) under the weak scattering, we obtain

$$\text{curl curl } \mathbf{E}^{\text{sc}} - \kappa^2 \mathbf{E}^{\text{sc}} = \kappa^2 q \mathbf{E}^{\text{in}}, \tag{24}$$

which is the well-known Born approximation.

Consider an auxiliary function

$$\mathbf{H}(\mathbf{x}) = \mathbf{b} e^{i\kappa \mathbf{x} \cdot \mathbf{d}},$$

where $\mathbf{b} \in \mathbb{S}^2$ is the polarization vector and $\mathbf{d} \in \mathbb{S}^2$ is the propagation direction with $\mathbf{b} \cdot \mathbf{d} = 0$. This function represents a propagating plane wave and hence satisfies Eq. (5). Multiplying Eq. (24) by \mathbf{H} and integrating over B on both sides, we have

$$\int_B (\text{curl curl } \mathbf{E}^{\text{sc}}) \cdot \mathbf{H} - \kappa^2 \int_B \mathbf{E}^{\text{sc}} \cdot \mathbf{H} = \kappa^2 \int_B q \mathbf{E}^{\text{in}} \cdot \mathbf{H}. \tag{25}$$

Integration by parts yields

$$\int_B (\text{curl curl } \mathbf{H}) \cdot \mathbf{E}^{\text{sc}} + \int_S [(\text{curl } \mathbf{H} \wedge \mathbf{n}) \cdot \mathbf{E}_S^{\text{sc}} - (\text{curl } \mathbf{E}^{\text{sc}} \wedge \mathbf{n}) \cdot \mathbf{H}_S] - \kappa^2 \int_B \mathbf{E}^{\text{sc}} \cdot \mathbf{H} = \kappa^2 \int_B q \mathbf{E}^{\text{in}} \cdot \mathbf{H}. \tag{26}$$

We have by noting Eq. (7) and the nonlocal boundary condition (9) that

$$\int_B q \mathbf{E}^{\text{in}} \cdot \mathbf{H} = \frac{1}{\kappa^2} \int_S [(\text{curl } \mathbf{H} \wedge \mathbf{n}) \cdot \mathbf{E}_S^{\text{sc}} - i\kappa \mathcal{T} \mathbf{E}_S^{\text{sc}} \cdot \mathbf{H}_S]. \tag{27}$$

It follows from the explicit form of the incident field and the auxiliary function that Eq. (27) can be deduced to

$$\int_B q(\mathbf{x}) e^{i(\mathbf{k} + \kappa \mathbf{d}) \cdot \mathbf{x}} = \frac{i}{(\mathbf{p} \cdot \mathbf{b}) \kappa} \int_S \{ [(\mathbf{d} \wedge \mathbf{b}) \wedge \mathbf{n}] \cdot \mathbf{E}_S^{\text{sc}} + [(\mathbf{b} \wedge \mathbf{n}) \wedge \mathbf{n}] \cdot \mathcal{T} \mathbf{E}_S^{\text{sc}} \} e^{i\kappa \mathbf{x} \cdot \mathbf{d}}. \tag{28}$$

As input data, the scattered field is available on S , so is its tangential component. Thus, the right hand of Eq. (28) may be defined as a known function $f(\eta, \mathbf{d})$. The linear integral equation (28) can be explicitly written as

$$\int_B q(\mathbf{x}) e^{i[(\eta_1 + \kappa d_1)x_1 + (\eta_2 + \kappa d_2)x_2]} e^{i(\kappa d_3 - \sqrt{\eta_1^2 + \eta_2^2 - \kappa^2})x_3} = f(\eta, \mathbf{d}), \tag{29}$$

which gives

$$\int_{-\infty}^{\infty} \hat{q}(\varrho, x_3) e^{i(\kappa d_3 - \sqrt{\eta_1^2 + \eta_2^2 - \kappa^2})x_3} = f(\eta, \mathbf{d}), \tag{30}$$

where $\varrho = (\eta_1 + \kappa d_1, \eta_2 + \kappa d_2)$ and $\hat{q}(\varrho, x_3)$ is the Fourier transform of $q(\mathbf{x})$ with respect to x_1 and x_2 . When the spatial frequency $|\eta|$ is large, the incident wave penetrates a thin layer of the scatterer. Thus, the Born approximation allows a reconstruction containing information of the true scatterer in that thin layer. When using propagating plane incident waves, the inversion involves data related to the scatterer through the Fourier transform in the case of weak scattering. However, when evanescent plane waves are used, the inversion involves data related to the scatterer through a Fourier (with respect to x_1 and x_2)–Laplace (with respect to x_3) transform in the case of the weak scattering.

Introduce the integral kernel

$$\mathcal{K}(\varrho; x_3) = e^{i(\kappa d_3 - \sqrt{\eta_1^2 + \eta_2^2 - \kappa^2})x_3}.$$

The integral equation (30) can be formally written as

$$\mathcal{K}(q)\hat{q}(q) = f(q), \tag{31}$$

which can be solved by using the method of least squares with Tikhonov regularization [19]

$$\hat{q}(q) = (\lambda\mathcal{I} + \mathcal{K}^*\mathcal{K})^{-1}\mathcal{K}^*f(q), \tag{32}$$

where λ is a small positive number, \mathcal{I} is the identity operator, and \mathcal{K}^* is the adjoint operator of \mathcal{K} . In practice, Eq. (32) is implemented by the LU-decomposition with partial pivoting. Once $\hat{q}(q, x_3)$ is available, an approximation of $q(\mathbf{x})$ may be obtained from the inverse Fourier transform, which leads to an initial approximation of the true scatterer.

Note 4. The linear integral equation (28) involves the scattered field on the whole sphere S , which requires the full aperture scattering data. When only limited aperture data are available, a similar linear integral equation could be deduced by using the fundamental solution of Maxwell's equations. Our numerical experiments exhibit the convergence based on initial guesses from the solutions of either one of the linear integral equations corresponding to full or limited aperture data.

4. Recursive linearization

As discussed in the previous section, when the spatial frequency $|\eta|$ is large, the Born approximation allows a reconstruction of the thin layer for the true scatterer. We now describe an iterative algorithm, which requires only single-frequency scattering data and is obtained by continuation on the spatial frequency of a two-parameter family of plane waves. The algorithm first solves the linearized integral equation (32) at a large spatial frequency to obtain an approximation of the scatterer. This approximation is then used to linearize the nonlinear equation with smaller spatial frequency of the incident waves, to produce a better approximation. The process is continued until the spatial frequency decreases to zero, where the approximation is considered as the final reconstruction.

Given the wavenumber κ , choose a positive number ϖ slightly larger than κ , and divide the interval $[0, \varpi]$ into N subdivisions with the endpoints $\{\varpi_0, \varpi_1, \dots, \varpi_N\}$, where $\varpi_0 = 0, \varpi_N = \varpi$, and $\varpi_{n-1} < \varpi_n$ for $1 \leq n \leq N$. We intend to obtain q_n recursively at $\varpi_n = \varpi_N, \varpi_{N-1}, \dots, \varpi_0$.

Suppose now that the scatterer q_{n+1} has been recovered at some ϖ_{n+1} and that ϖ_n is slightly less than ϖ_{n+1} . We wish to determine q_n , or equivalently, to determine the perturbation

$$\delta q = q_n - q_{n+1}.$$

For the reconstructed scatterer $q_{n+1} = q_{n+1}^1$, we solve the direct scattering problem

$$\text{curl curl } \tilde{\mathbf{E}}_m^{\text{sc}} - \kappa^2(1 + q_{n+1}^m)\tilde{\mathbf{E}}_m^{\text{sc}} = \kappa^2 q_{n+1}^m \mathbf{E}_m^{\text{in}} \quad \text{in } B, \tag{33}$$

$$\text{curl } \tilde{\mathbf{E}}_m^{\text{sc}} \wedge \mathbf{n} - i\kappa\mathcal{T}\tilde{\mathbf{E}}_{mS}^{\text{sc}} = \mathbf{0} \quad \text{on } S, \tag{34}$$

where the incident wave $\mathbf{E}_m^{\text{in}} = \mathbf{p}e^{i\mathbf{k}\cdot\mathbf{x}}$, the wave vector $\mathbf{k} = (\eta_m, k(\eta_m))$, and the transverse wave vector $\eta_m = (\varpi_n \cos\theta_m, \varpi_n \sin\theta_m)$, $\theta_m \in [0, 2\pi]$, $m = 1, \dots, M$.

For the scatterer q_n , we have

$$\text{curl curl } \mathbf{E}_m^{\text{sc}} - \kappa^2(1 + q_n)\mathbf{E}_m^{\text{sc}} = \kappa^2 q_n \mathbf{E}_m^{\text{in}} \quad \text{in } B, \tag{35}$$

$$\text{curl } \mathbf{E}_m^{\text{sc}} \wedge \mathbf{n} - i\kappa\mathcal{T}\mathbf{E}_{mS}^{\text{sc}} = \mathbf{0} \quad \text{on } S. \tag{36}$$

Subtracting Eqs. (33) and (34) from Eqs. (35) and (36) respectively, and omitting the second order smallness in $\delta q^m = q_n - q_{n+1}^m$ and in $\delta \mathbf{E}_m^{\text{sc}} = \mathbf{E}_m^{\text{sc}} - \tilde{\mathbf{E}}_m^{\text{sc}}$, we obtain

$$\text{curl curl } \delta \mathbf{E}_m^{\text{sc}} - \kappa^2(1 + q_{n+1}^m)\delta \mathbf{E}_m^{\text{sc}} = \kappa^2 \delta q^m (\mathbf{E}_m^{\text{in}} + \tilde{\mathbf{E}}_m^{\text{sc}}) \quad \text{in } B, \tag{37}$$

$$\text{curl } \delta \mathbf{E}_m^{\text{sc}} \wedge \mathbf{n} - i\kappa\mathcal{T}\delta \mathbf{E}_{mS}^{\text{sc}} = \mathbf{0} \quad \text{on } S. \tag{38}$$

Given a solution \mathbf{E}_m^{sc} of Eqs. (35) and (36), we define the measurements

$$\mathcal{M}\mathbf{E}_m^{\text{sc}}(\mathbf{x}) = [\mathbf{E}_m^{\text{sc}}(\mathbf{x}_1), \dots, \mathbf{E}_m^{\text{sc}}(\mathbf{x}_j)]. \tag{39}$$

The measurement operator \mathcal{M} is well defined and maps the scattered field to a vector of complex numbers in \mathbb{C}^J , which consists of point measurements of the scattered field at $\mathbf{x}_j, j = 1, \dots, J$.

For the scatterer q_n and the incident field \mathbf{E}_m^{in} , we define the forward scattering operator

$$\mathcal{S}(q_n, \mathbf{E}_m^{\text{in}}) = \mathcal{M}\mathbf{E}_m^{\text{sc}}. \tag{40}$$

It is easily seen that the forward scattering operator $\mathcal{S}(q_n, \mathbf{E}_m^{\text{in}})$ is linear with respect to \mathbf{E}_m^{in} but nonlinear with respect to q_n . For simplicity, we denote $\mathcal{S}(q_n, \mathbf{E}_m^{\text{in}})$ by $S_m(q_n)$. Let $\mathcal{S}'(q_{n+1}^m)$ be the Fréchet derivative of $S_m(q_n)$ and denote the residual operator

$$\mathcal{R}(q_{n+1}^m) = \mathcal{M}(\delta \mathbf{E}_m^{\text{sc}}). \tag{41}$$

It follows from the linearization of the nonlinear equation (40) that

$$S'(q_{n+1}^m) \delta q^m = \mathcal{R}(q_{n+1}^m). \tag{42}$$

Applying the Landweber–Kaczmarz iteration [27] to the linearized equation (42) yields

$$\delta q^m = \alpha S'(q_{n+1}^m)^* \mathcal{R}(q_{n+1}^m) \quad \text{for } m = 1, \dots, M, \tag{43}$$

where α is a positive relaxation parameter and $S'(q_{n+1}^m)^*$ is the adjoint operator of $S'(q_{n+1}^m)$. The Landweber–Kaczmarz method usually displays better convergence property than the simple Landweber iteration [23,31]. The relation between the Landweber iteration and Landweber–Kaczmarz is of the same type as between the Jacobi and Gauss–Seidel iteration for linear systems.

In order to compute the correction δq^m , we need an efficient way to compute $S'(q_{n+1}^m)^* \mathcal{R}(q_{n+1}^m)$. Let $\mathcal{R}(q_{n+1}^m) = [\phi_{m1}, \dots, \phi_{mj}]^T \in \mathbb{C}^{3J}$. Consider the adjoint problem

$$\text{curl curl } \mathbf{W}_m - \kappa^2(1 + q_{n+1}^m) \mathbf{W}_m = \kappa^2 \sum_{j=1}^J \phi_{mj} \delta(\mathbf{x} - \mathbf{x}_j) \quad \text{in } B, \tag{44}$$

$$\text{curl } \mathbf{W}_m \wedge \mathbf{n} - i\kappa \mathcal{T}^* \mathbf{W}_m \mathcal{S} = 0 \quad \text{on } S, \tag{45}$$

where \mathcal{T}^* is the adjoint capacity operator of \mathcal{T} , defined as

$$\mathcal{T}^* \mathbf{u} = - \sum_{n=1}^{\infty} \sum_{m=-n}^n \left[\frac{\alpha_n^m \bar{\gamma}_n(\kappa)}{i\kappa} \mathbf{U}_n^m + \frac{i\kappa \beta_n^m}{\bar{\gamma}_n(\kappa)} \mathbf{V}_n^m \right].$$

Multiplying Eq. (37) by the complex conjugate of \mathbf{W}_m and integrating over B on both sides, we obtain

$$\int_B (\text{curl curl } \delta \mathbf{E}_m^{\text{sc}}) \cdot \bar{\mathbf{W}}_m - \int_B \kappa^2 (\mathbf{1} + \mathbf{q}_{n+1}^m) \delta \mathbf{E}_m^{\text{sc}} \cdot \bar{\mathbf{W}}_m = \kappa^2 \int_B \delta \mathbf{q}^m (\mathbf{E}_m^{\text{in}} + \tilde{\mathbf{E}}_m^{\text{sc}}) \cdot \bar{\mathbf{W}}_m.$$

Using Green’s formula, we have

$$\begin{aligned} & \int_B (\text{curl curl } \bar{\mathbf{W}}_m - \kappa^2 (\mathbf{1} + \mathbf{q}_{n+1}^m) \bar{\mathbf{W}}_m) \cdot \delta \mathbf{E}_m^{\text{sc}} + \int_S [(\text{curl } \bar{\mathbf{W}} \wedge \mathbf{n}) \cdot \delta \mathbf{E}_m^{\text{sc}} - (\text{curl } \delta \mathbf{E}_m^{\text{sc}} \wedge \mathbf{n}) \cdot \bar{\mathbf{W}}_m] \\ & = \kappa^2 \int_B \delta \mathbf{q}^m (\mathbf{E}_m^{\text{in}} + \tilde{\mathbf{E}}_m^{\text{sc}}) \cdot \bar{\mathbf{W}}_m. \end{aligned}$$

It follows from the adjoint Eq. (44) that

$$\sum_{j=1}^J \delta \mathbf{E}_m^{\text{sc}}(\mathbf{x}_j) \bar{\phi}_{mj} = \int_B \delta q^m (\mathbf{E}_m^{\text{in}} + \tilde{\mathbf{E}}_m^{\text{sc}}) \cdot \bar{\mathbf{W}}_m. \tag{46}$$

Noting Eqs. (39), (41), and the adjoint operator $S'(q_{\eta}^m)^*$, the left-hand side of Eq. (46) may be deduced

$$\begin{aligned} & \sum_{j=1}^J \delta \mathbf{E}_m^{\text{sc}}(\mathbf{x}_j) \bar{\zeta}_{mj} = \langle \mathcal{M}(\delta \mathbf{E}_m^{\text{sc}}), \mathcal{R}(q_{n+1}^m) \rangle_{\mathbb{C}^{3J}} = \langle S'(q_{n+1}^m) \delta q^m, \mathcal{R}(q_{n+1}^m) \rangle_{\mathbb{C}^{3J}} = \langle \delta q^m, S'(q_{n+1}^m)^* \mathcal{R}(q_{n+1}^m) \rangle_{L^2(B)} \\ & = \int_B \delta q^m \overline{S'(q_{n+1}^m)^* \mathcal{R}(q_{n+1}^m)}, \end{aligned} \tag{47}$$

where $\langle \cdot, \cdot \rangle_{\mathbb{C}^{3J}}$ and $\langle \cdot, \cdot \rangle_{L^2(B)}$ are the standard inner-products defined in the complex vector space \mathbb{C}^{3J} and the square integrable functional space $L^2(B)$.

Combining Eqs. (46) and (47) yields

$$\int_B \delta q^m \overline{S'(q_{n+1}^m)^* \mathcal{R}(q_{n+1}^m)} = \int_B \delta q^m (\mathbf{E}_m^{\text{in}} + \tilde{\mathbf{E}}_m^{\text{sc}}) \cdot \bar{\mathbf{W}}_m,$$

which holds for any δq^m . It follows that

$$S'(q_{n+1}^m)^* \mathcal{R}(q_{n+1}^m) = \overline{(\mathbf{E}_m^{\text{in}} + \tilde{\mathbf{E}}_m^{\text{sc}})} \cdot \mathbf{W}_m. \tag{48}$$

Using the above result, Eq. (43) can be written as

$$\delta q^m = \alpha \overline{(\mathbf{E}_m^{\text{in}} + \tilde{\mathbf{E}}_m^{\text{sc}})} \cdot \mathbf{W}_m \quad \text{for } m = 1, \dots, M. \tag{49}$$

Thus, for each incident wave, we solve one direct problem (35) and one adjoint problem (44). Once δq^m is determined, q_{n+1}^{m+1} is updated by $q_{n+1}^m + \delta q^m$. After completing the M th sweep, we get the reconstructed scatterer $q_n = q_{n+1}^M$ at the spatial frequency ϖ_n .

5. Numerical experiments

In this section, we discuss the numerical solution of the direct scattering problem and the computational issues of the recursive linearization algorithm.

For the direct solver, we adopt the edge elements which were developed originally for the finite element solution of Maxwell's equation in the early 1980s [36]. From a mathematical point of view, these are natural approximation spaces of the Hilbert space $H(\text{curl}, B)$ which is the adequate functional space for the variational formulation of Maxwell's equations. Vector fields in such a finite element space have continuous tangential traces, which is consistent with the physics. Therefore, the natural degrees of freedom for these elements are related to tangential traces along the edges or faces. Although the direct scattering problem may be formulated in a bounded ball with exact boundary condition (8) and (9), the discretization of the nonlocal boundary condition (9) would lead to some extra difficulty because the lack of the sparsity of the linear system. For the sake of simplicity, we employ a local absorbing boundary condition [26]

$$\text{curl} \mathbf{E}^{\text{sc}} \wedge \mathbf{n} - i\kappa \mathbf{E}_S^{\text{sc}} = 0 \quad \text{on } S.$$

Creating a mesh is the first step in the finite element method. We use a simple and effective mesh generator in MATLAB by Persson and Strang [38]. Once the mesh generation is done and node information is available, we convert it into the edge information because unknowns are associated with edges. When the unknowns are ordered according to the reverse Cuthill–McKee ordering [21], the profile of the finite element matrix is highly banded, which improves the condition number of the corresponding coefficient matrix. The sparse large scale linear system can be efficiently solved if the zero elements of the coefficient matrix are not stored. We use the compressed row storage format, which makes no assumptions about the sparsity structure of the matrix and does not store any unnecessary elements. In fact, from the variational formula of the direct problem, the coefficient matrix is complex symmetric. Hence, only the lower triangular portion of the matrix needs to be stored. Regarding the linear solver, the quasi-minimal residual algorithm [20] with the incomplete LU-decomposition preconditioning is used to solve the sparse, symmetric, and complex system of the equations.

In the following, some numerical experiments are presented to illustrate the performance of the algorithm. To get the initial guesses, the integral in Eq. (30) is discretized by using the composite trapezoidal rule and the regularization λ is taken as 10^{-5} . In the recursive linearization iteration, the relaxation parameter is taken to be $0.01/\kappa^2$, which is independent of the spatial frequency. For stability analysis, some relative random noise is added to the data, *i.e.*, the scattered field takes the form

$$\mathbf{E}^{\text{sc}}(\mathbf{x}_j) := (1 + \sigma \text{rand}) \mathbf{E}^{\text{sc}}(\mathbf{x}_j), \quad j = 1, \dots, J.$$

Here, rand gives uniformly distributed random number in $[-1, 1]$, σ is a noise level parameter, and the sweep number M at each spatial frequency is 10 in the implementation. Define the relative error by

$$\frac{(\sum_{\text{edge}} |q_{\text{edge}} - \tilde{q}_{\text{edge}}|^2)^{1/2}}{(\sum_{\text{edge}} |q_{\text{edge}}|^2)^{1/2}},$$

where \tilde{q} is the reconstructed scatterer and q is the true scatterer. To avoid the inverse crime being committed, we made sure that different meshes were used for the forward and inverse computations. Finally, since we can only plot slices of the graphs for three-dimensional functions, we have to interpolate the edge values from tetrahedra of the reconstructed scatterer into the Cartesian grid.

Let $q(x_1, x_2, x_3) = \exp(-x_1^2 - x_2^2 - x_3^2)$, and reconstruct the scatterer defined by

$$q_1(x_1, x_2, x_3) = q(2.5x_1, 3.5x_2, 2.5x_3).$$

See Fig. 1 for graphs of the true scatterer at slices $x_1 = 0.3$, $x_2 = 0$, and $x_3 = 0$. This function is difficult to reconstruct because of two close peaks. The wavenumber κ is taken as 2π , the maximum spatial frequency $\varpi = 8$, the step size of $\Delta\varpi = 2$, and a

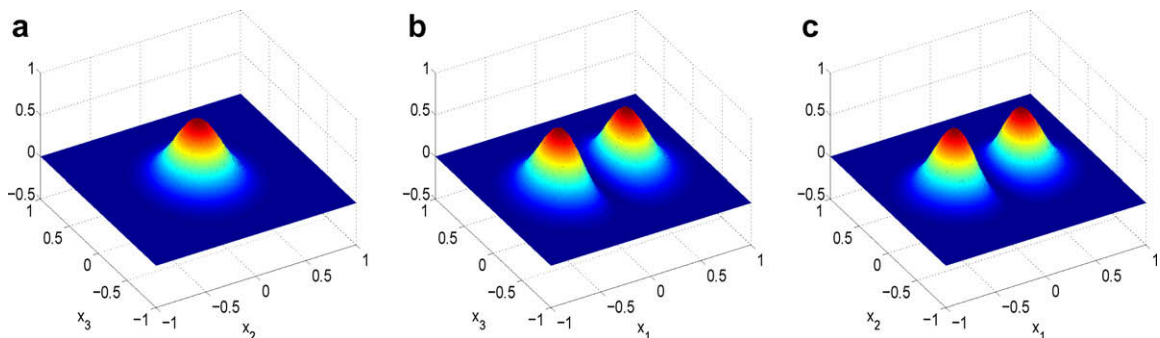


Fig. 1. The true scatterer. (a): the slice $x_1 = 0.3$; (b): the slice $x_2 = 0$; (c): the slice $x_3 = 0$.

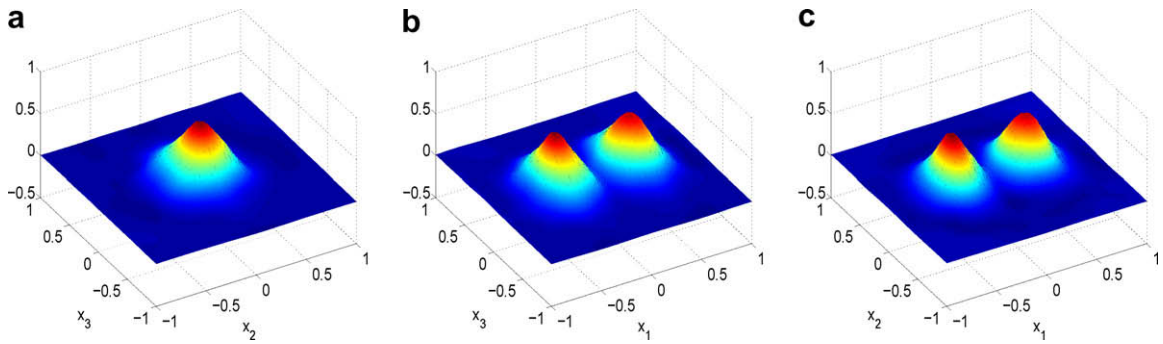


Fig. 2. The reconstructed scatterer with full aperture data. (a): the slice $x_1 = 0.3$; (b): the slice $x_2 = 0$; (c): the slice $x_3 = 0$.

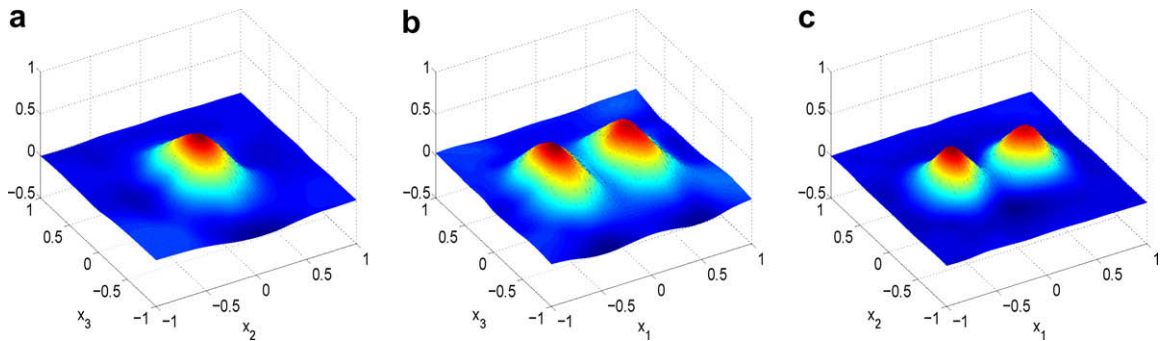


Fig. 3. The reconstructed scatterer with limited aperture data. (a): the slice $x_1 = 0.3$; (b): the slice $x_2 = 0$; (c): the slice $x_3 = 0$.

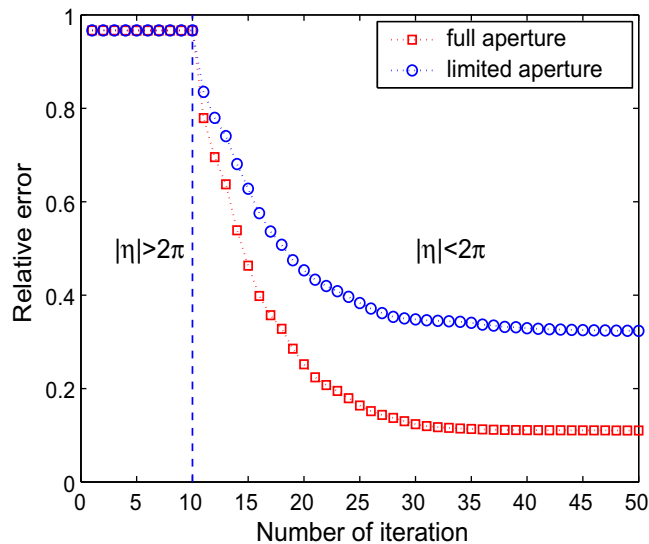


Fig. 4. The relative error of reconstruction with full and limited aperture data. The first 10 iterations corresponds to evanescent incident plane waves ($|\eta| > \kappa = 2\pi$), and the rest 40 iterations corresponds to propagating incident plane waves ($|\eta| < \kappa = 2\pi$).

noise level parameter $\sigma = 0.05$. Figs. 2 and 3 show the reconstructed scatterer at different slices using the full aperture data and limited aperture data (upper part of the sphere), respectively. Fig. 4 plots the relative error of reconstruction as a function of iteration numbers for full and limited aperture cases. As expected, the error of reconstruction with full aperture data is small than that with limited aperture data. The first 10 iterations correspond to the evanescent incident plane waves ($|\eta| > \kappa = 2\pi$) and the rest 40 iterations correspond to the propagating incident plane waves ($|\eta| < \kappa = 2\pi$). Although it seems that the evanescent incident plane waves do not contribute much to the accuracy of reconstructions, the initial guesses, which are derived from the weak scattering due to them, lead to the convergence of the algorithm.

6. Conclusion

We have presented a regularized recursive linearization method with respect to the spatial frequency of a two-family plane waves. This approach extends the one proposed in [4] for solving the two-dimensional Helmholtz equation to the three-dimensional Maxwell's equation at fixed frequency. The method is stable and efficient, and can be used to deal with the limited aperture case. Finally, we point out some future directions along the line of this work. The first is concerned with the convergence analysis. Although our numerical experiments demonstrate the convergence and stability of the inversion algorithm, no rigorous mathematical result is available at present. Initial attempt has been made recently in [8] to establish convergence results by taking into account of the uncertainty principle. Another direction is to investigate the half space geometry instead of the free space. In this paper, we overlook the effect of the other medium on the detected scattered field. In practice, however, it is important to include the effect of the other medium and even the tip, especially for near-field optics.

References

- [1] H. Ammar, G. Bao, Maxwell's equations in periodic chiral structures, *Math. Nachr.* 251 (2003) 3–18.
- [2] H. Ammari, J. Nédélec, Low-frequency electromagnetic scattering, *SIAM J. Math. Anal.* 31 (2000) 836–861.
- [3] G. Bao, P. Li, Inverse medium scattering problems for electromagnetic waves, *SIAM J. Appl. Math.* 65 (2005) 2049–2066.
- [4] G. Bao, P. Li, Inverse medium scattering for the Helmholtz equation at fixed frequency, *Inv. Probl.* 21 (2005) 1621–1641.
- [5] G. Bao, P. Li, Numerical solution of inverse scattering for near-field optics, *Optics Lett.* 32 (2007) 1465–1467.
- [6] G. Bao, P. Li, Inverse medium scattering problem in near-field optics, *J. Comp. Math.* 25 (2007) 252–265.
- [7] G. Bao, J. Liu, Numerical solution of inverse problems with multi-experimental limited aperture data, *SIAM J. Sci. Comput.* 25 (2003) 1102–1117.
- [8] G. Bao, F. Triki, Error estimates of the recursive linearization for inverse medium problems, preprint.
- [9] P. Carney, J. Schotland, Three-dimensional total internal reflection microscopy, *Opt. Lett.* 26 (2001) 1072–1074.
- [10] P. Carney, J. Schotland, Near-field tomography, *MSRI Ser. Math. Appl.* 47 (2003) 131–166.
- [11] Y. Chen, Inverse scattering via Heisenberg uncertainty principle, *Inv. Probl.* 13 (1997) 253–282.
- [12] Y. Chen, Inverse scattering via skin effect, *Inv. Probl.* 13 (1997) 649–667.
- [13] W. Chew, Y. Wang, Reconstruction of two-dimensional permittivity distribution using the distorted Born iteration method, *IEEE Trans. Med. Imaging* 9 (1990) 218–225.
- [14] D. Colton, R. Kress, *Inverse Acoustic and Electromagnetic Scattering Theory*, Applied Mathematics Science, second ed., vol. 93, Springer-Verlag, Berlin, 1998.
- [15] D. Colton, J. Coyle, P. Monk, Recent development in inverse acoustic scattering theory, *SIAM Rev.* 42 (2000) 369–414.
- [16] D. Courjon, *Near-Field Microscopy and Near-Field Optics*, Imperial College press, London, 2003.
- [17] D. Courjon, C. Bainier, Near field microscopy and near field optics, *Rep. Prog. Phys.* 57 (1994) 989–1028.
- [18] O. Dorn, H. Bertete-Aguirre, J.G. Berrymann, G.C. Papanicolaou, A nonlinear inversion method for 3D electromagnetic imaging using adjoint fields, *Inv. Probl.* 15 (1999) 1523–1558.
- [19] H. Engl, M. Hanke, A. Neubauer, *Regularization of Inv. Problems*, Kluwer, Dordrecht, 1996.
- [20] R. Freund, A transpose-free quasi-minimum residual algorithm for non-Hermitian linear systems, *SIAM J. Sci. Comput.* 14 (1993) 470–482.
- [21] N. Gibbs, W. Poole Jr., P. Stockmeyer, An algorithm for reducing the bandwidth and profile of a sparse matrix, *SIAM J. Numer. Anal.* 13 (1976) 236–250.
- [22] C. Girard, A. Dereux, Near-field optics theories, *Rep. Prog. Phys.* 59 (1996) 657–699.
- [23] M. Hanke, A. Neubauer, O. Scherzer, A convergence analysis of the Landweber iteration for nonlinear ill-posed problems, *Numer. Math.* 72 (1995) 21–37.
- [24] T. Hohage, On the numerical solution of a three-dimensional inverse medium scattering problem, *Inv. Probl.* 17 (2001) 1743–1763.
- [25] T. Hohage, Fast numerical solution of the electromagnetic medium scattering problem and applications to the inverse problem, *J. Comput. Phys.* 214 (2006) 224–238.
- [26] J. Jin, *The Finite Element Methods in Electromagnetics*, John Wiley & Sons, 2002.
- [27] B. Kaltenbacher, A. Neubauer, O. Scherzer, Convergence of projected iterative regularization methods for nonlinear problems with smooth solutions, *Inv. Probl.* 22 (2006) 1105–1119.
- [28] A. Kirsch, P. Monk, A finite element/spectral method for approximating the time-harmonic Maxwell's system in \mathbb{R}^3 , *SIAM J. Appl. Math.* 55 (1995) 1324–1344.
- [29] A. Kirsch, P. Monk, Corrigendum: A finite element/spectral method for approximating the time-harmonic Maxwell's system in \mathbb{R}^3 , *SIAM J. Appl. Math.* 58 (1999) 2024–2028.
- [30] A. Kirsch, P. Monk, A finite element method for approximating electro-magnetic scattering from a conducting object, *Numer. Math.* 92 (2002) 501–534.
- [31] R. Kowar, O. Scherzer, Convergence analysis of a Landweber–Kaczmarz method for solving nonlinear ill-posed problems, in: S. Romanov, S.I. Kabanikhin, Y.E. Anikonov, A.L. Bukhgeim (Eds.), *Ill-posed and Inverse Problems*, VSP Publishers, Zeist, 2002.
- [32] P. Monk, *Finite Element Methods for Maxwell's Equations*, Oxford University Press, Oxford, UK, 2003.
- [33] F. Natterer, *The Mathematics of Computerized Tomography*, Teubner, Stuttgart, 1986.
- [34] F. Natterer, F. Wübbeling, A propagation–backpropagation method for ultrasound tomography, *Inv. Probl.* 11 (1995) 1225–1232.
- [35] F. Natterer, F.F. Wübbeling, Marching schemes for inverse acoustic scattering problems, *Numer. Math.* 100 (2005) 697–710.
- [36] J. Nédélec, Mixed finite element in \mathbb{R}^3 , *Numer. Math.* 35 (1980) 315–341.
- [37] J. Nédélec, *Acoustic and Electromagnetic Equations: Integral Representations for Harmonic Problems*, Springer, New York, 2000.
- [38] P. Persson, G. Strang, A simple mesh generator in Matlab, *SIAM Rev.* 46 (2004) 329–345.
- [39] M. Vögeler, Reconstruction of the three-dimensional refractive index in electromagnetic scattering using a propagation–backpropagation method, *Inv. Probl.* 19 (2003) 739–753.